

**Fully nonperturbative charm-quark tuning using machine learning**R. J. Hudspith<sup>\*</sup>*PRISMA+ Cluster of Excellence and Institut für Kernphysik, Johannes Gutenberg-Universität Mainz,  
55099 Mainz, Germany*D. Mohler<sup>†</sup>*GSI Helmholtzzentrum für Schwerionenforschung, 64291 Darmstadt, Germany*

(Received 13 January 2022; accepted 26 July 2022; published 18 August 2022)

We present a relativistic heavy-quark action tuning for the charm sector on ensembles generated by the Coordinated Lattice Simulations consortium. We tune a particular five-parameter action in an entirely nonperturbative and—up to the chosen experimental input—model-independent way using machine learning and the continuum experimental charmonium ground-state masses with various quantum numbers. In the end, we are reasonably successful; obtaining a set of simulation parameters that we then verify produces the expected spectrum. In the future, we will use this action for finite-volume calculations of hadron-hadron scattering.

DOI: [10.1103/PhysRevD.106.034508](https://doi.org/10.1103/PhysRevD.106.034508)**I. MOTIVATION**

In recent years, studies of hadron-hadron scattering using Lüscher's finite-volume method [1,2] have become the state of the art for obtaining information about physical scattering amplitudes from lattice QCD. In the light-quark sector, such studies typically make use of moving frames to maximize the information about scattering amplitudes deduced from a single gauge-field ensemble (for examples, please refer to Ref. [3]).

For hadrons with heavy charm or bottom quarks, keeping heavy-quark discretization effects under control is an additional concern. In the case of ensembles generated by the Coordinated Lattice Simulations (CLS) consortium [4], using the same Wilson-clover action [5] for heavy quarks as is used for light (up, down, and strange) quarks, leads to sizable heavy-quark discretization effects [6] for all but the finest lattice spacings considered. These discretization effects can be understood in the context of the Fermilab approach [7,8]. In one of the standard implementations used extensively by the Fermilab Lattice and MILC Collaborations (see, for example, [9–11]), a single parameter of the relativistic heavy-quark (RHQ) action discussed in the next section is tuned nonperturbatively. This approach was used

for the study of hadron resonances and bound states with Lüscher's finite-volume method, to study heavy-light mesons [12–14] and charmonium [15]. However, tuning only a single parameter nonperturbatively, significant discretization effects are still present in hadronic dispersion relations [8,13], which complicates the change of frame from interacting two-hadron energies in moving frames to the center-of-momentum frame needed to make use of moving frames in the scattering calculation. For this reason, only rest-frame data were used in Refs. [12–15]. In more recent studies of the charmonium spectrum in (coupled-channel) scattering of charmed mesons [16,17], moving frames were used by extracting energy differences with regard to only close-by noninteracting meson-meson levels and by purely working with the continuum form of the dispersion relations, which minimizes the effects from heavy-quark discretization effects [18]. This introduces a hard-to-quantify systematic uncertainty.

In heavy-hadron spectroscopy studies pursued by the Hadron Spectrum Collaboration, anisotropic lattices are used to study multihadron scattering with heavy hadrons [19–23]. In their approach, the fine temporal lattice spacing combined with a tuning of the mass and anisotropy parameters that reproduce the physical  $\eta_c$  mass and a relativistic dispersion relation enable the use of moving frames. Discretization effects in the spin-dependent splittings are still, however, expected to be sizable in such an approach [8].

To reduce the uncertainty from heavy-quark discretization effects in the context of scattering studies, it is therefore desirable to at least tune the dispersion relation to be approximately relativistic with a speed of light  $c = 1$  (in natural units). In the next section, we will introduce the relativistic heavy-quark action used. We then proceed to

<sup>\*</sup>renwick.james.hudspith@googlemail.com<sup>†</sup>d.mohler@gsi.de

*Published by the American Physical Society under the terms of the Creative Commons Attribution 4.0 International license. Further distribution of this work must maintain attribution to the author(s) and the published article's title, journal citation, and DOI. Funded by SCOAP<sup>3</sup>.*

describe the lattice gauge-field ensembles used in our simulation and to describe the methodology for a fully nonperturbative tuning of this action. In Sec. IV, we proceed to show the outcome of this tuning procedure and compare it to the charm simulations with the CLS light-quark action. In Sec. V, we summarize our results and provide a brief outlook.

## II. INTRODUCTION

While the Fermilab approach already appeared in Ref. [7], we will more closely follow Refs. [24,25], also known in the literature as the ‘‘Tsukuba’’ action, and write down a general asymmetric Wilson action:

$$\begin{aligned}
 D_{xy} = & \delta_{xy} \\
 & -\kappa_c \left[ \sum_i (r_s - \nu\gamma_i) U_i(x) \delta_{x+i,y} + (r_s + \nu\gamma_i) U_i^\dagger(x) \delta_{x,y+i} \right] \\
 & -\kappa_c [(r_t - \gamma_t) U_t(x) \delta_{x+t,y} + (r_t + \gamma_t) U_t^\dagger(x) \delta_{x,y+t}] \\
 & -\kappa_c \left[ c_B \sum_{i,j} \sigma_{ij} F_{ij}(x) + c_E \sum_i \sigma_{ii} F_{ii}(x) \right] \delta_{xy}. \quad (1)
 \end{aligned}$$

Commonly,  $r_t = 1$  is chosen, as this parameter is argued to be redundant. The remaining five parameters are  $\kappa_c$ ,  $r_s$ ,  $\nu$ ,  $c_E$ , and  $c_B$ . Prescriptions in the literature exist for choosing these parameters based on mean-field-improved perturbation theory and for nonperturbative tuning of individual parameters. An in-depth discussion about our implementation of this action within the library openQCD can be found in Appendix A. We would like to make it clear that our methodology does not rely on this specific choice of action and could be simply applied to any of the tunings employed in the literature.

In Refs. [9–11],  $c_{\text{SW}} = c_E = c_B \equiv u_0^{-3}$  is set to the value from tree-level tadpole-improved perturbation theory, with the tadpole factor  $u_0$  determined from the fourth root of the plaquette, or the mean Landau link. In addition, the choices  $r_s = \nu = 1$  are used. Note that it is argued that  $r_s$  is a redundant parameter. In this approach, only  $\kappa_c$  is determined nonperturbatively (from tuning the kinetic mass  $M_2$  of the  $D_s$  meson to its physical value). In the context of spectroscopy, this approach was used in Ref. [26] to obtain an excellent description of ground-state mass splittings in the charmonium spectrum. In the Fermilab approach [7,8,27], the heavy-meson dispersion relations take the general form

$$E(p) = M_1 + \frac{p^2}{2M_2} - \frac{(p^2)^2}{8M_4^3} - \frac{a^3 W_4}{6} \sum_i p_i^4 + \dots, \quad (2)$$

due to broken Lorentz symmetry.  $M_1$  is known as the (meson) rest mass and  $M_2$  as the kinetic mass, and  $M_4$  and higher are referred to as generalized masses [27]. The term

with  $W_4$  and similar higher-order terms occur due to rotational symmetry breaking, and, in general,  $M_1 \neq M_2 \neq M_4 \dots$ . When tuning only  $\kappa_c$ , the resulting sizable difference between  $M_1$  and  $M_2$  is of concern for the scattering studies detailed in Sec. I.

In Ref. [25], the specific five-parameter action of Eq. (1) was introduced. In Refs. [28–30], this action was *semi-nonperturbatively* tuned on a set of ensembles with the same lattice spacing  $a^{-1} = 2.194(10)$  GeV, where  $\kappa_c$  was tuned to obtain the physical spin average of the  $\eta_c$  and  $J/\psi$  masses. The parameter  $r_s$  was determined completely perturbatively using one-loop mean-field-improved expressions, whereas  $c_E$  and  $c_B$  were determined from perturbative mass corrections to the nonperturbatively measured  $c_{\text{SW}}$  of Ref. [32]. The value of  $\nu$  was tuned independently of all the other parameters to obtain the relativistic dispersion relation  $c^2 = 1$ . We will discuss such an approach later in Sec. IV B, as we allow all parameters to vary and can infer their interdependence. Having  $c^2 = 1$  is quite useful, as we will not have to determine masses of states through their dispersion relation; in the Fermilab language, we are enforcing that  $M_1 = M_2$ .

Finally, in Ref. [33], a more conventional fully nonperturbative tuning of the four-parameter action with  $r_t = 1$  and  $r_s = \nu$  and of the three-parameter action where, additionally,  $c_E = c_B$  has been performed [34], also allowing  $M_1 = M_2$ . Here, the argument that  $c_E = c_B$  can be chosen relied on the observation of nonstable parameters when performing the tuning of the four-parameter action in Ref. [33]. In a companion paper [36], it was argued (in their RHQ power counting) that this was a consequence of  $c_B - c_E$  being redundant up to higher-order effects.

For our own study, we keep all five parameters. Before introducing the details of our methodology, we would like to point out that  $c_E \approx c_B$  indeed results from our tuning, and—insofar as this can be seen on our limited range of lattice spacings—both values slowly approach  $c_{\text{SW}}$ , while  $\nu$  and  $r_s$  approach  $1 = r_t$ . In particular, in contrast to Ref. [33], we do not observe any instabilities in our predictions across different ensembles or lattice spacings, and all five parameters will be reasonably well determined.

## III. METHODOLOGY

### A. Gauge-field ensembles

We perform calculations on gauge-field ensembles generated by the CLS consortium [4,37] with  $2 + 1$  flavors of dynamical, nonperturbatively improved Wilson fermions [5]. We use five different lattice spacings ranging from  $a = 0.09929$  to  $0.04981$  fm, and with pion masses between 421 and 282 MeV, on trajectories where the trace of the quark mass matrix  $\text{Tr } M$  is kept constant and approximately physical. In our study, we use ensembles with either open [38] or periodic boundary conditions in time. The ensembles we considered for the tuning of the relativistic heavy-quark action are listed in Table I.

TABLE I. Table of ensembles—values for the lattice spacing come from Refs. [6,39], as do the pion masses. Further details on these ensembles can be found in Ref. [4]. Here,  $N_{\text{conf}}$  indicates the number of well-separated gauge configurations used and  $N_{\text{src}}$  the number of time-translated wall sources averaged over per gauge configuration.

$\beta$	Name	$L^3 \times L_T$	$T$ boundary	$N_{\text{conf}} \times N_{\text{src}}$	$a^{-1}$ [GeV]	$m_\pi$ [GeV]
3.34	A653	$24^3 \times 48$	Periodic	$100 \times 16$	1.987(20)	0.422(4)
3.34	A654	$24^3 \times 48$	Periodic	$100 \times 16$	1.987(20)	0.331(3)
3.40	U103	$24^3 \times 128$	Open	$1000 \times 1$	2.285(28)	0.419(5)
3.40	H101	$32^3 \times 96$	Open	$500 \times 1$	2.285(28)	0.416(5)
3.40	H102	$32^3 \times 96$	Open	$500 \times 1$	2.285(28)	0.354(5)
3.40	H105	$32^3 \times 96$	Open	$500 \times 1$	2.285(28)	0.284(4)
3.46	B450	$32^3 \times 64$	Periodic	$100 \times 16$	2.585(33)	0.416(4)
3.46	S400	$32^3 \times 128$	Open	$500 \times 1$	2.585(33)	0.351(4)
3.46	N451	$48^3 \times 128$	Periodic	$253 \times 8$	2.585(33)	0.287(4)
3.55	H200	$32^3 \times 96$	Open	$1000 \times 1$	3.071(36)	0.419(5)
3.55	N202	$48^3 \times 128$	Open	$900 \times 1$	3.071(36)	0.410(5)
3.55	N203	$48^3 \times 128$	Open	$750 \times 1$	3.071(36)	0.345(4)
3.55	N200	$48^3 \times 128$	Open	$856 \times 1$	3.071(36)	0.282(3)
3.70	N300	$48^3 \times 128$	Open	$770 \times 1$	3.962(45)	0.421(4)

## B. Obtaining the dispersion relation

We will follow Appendix A of Ref. [40] [in that context used for tuning a nonrelativistic quantum chromodynamics (NRQCD) action] and use partially twisted Coulomb-gauge-fixed wall sources [41] to determine the spin-averaged dispersion relation of the  $\eta_c$  and  $J/\psi$ . We will partially twist [43,44] along the diagonal  $(\theta, \theta, \theta)$  to maximally reduce effects from rotational symmetry breaking and use the following five twist angles (in lattice units):

$$\theta_i = 0, \sqrt{\frac{2}{9}}, \sqrt{\frac{4}{9}}, \sqrt{\frac{6}{9}}, \sqrt{\frac{8}{9}},$$

such that our values of  $(ap)^2$  are evenly distributed between 0 and 3.

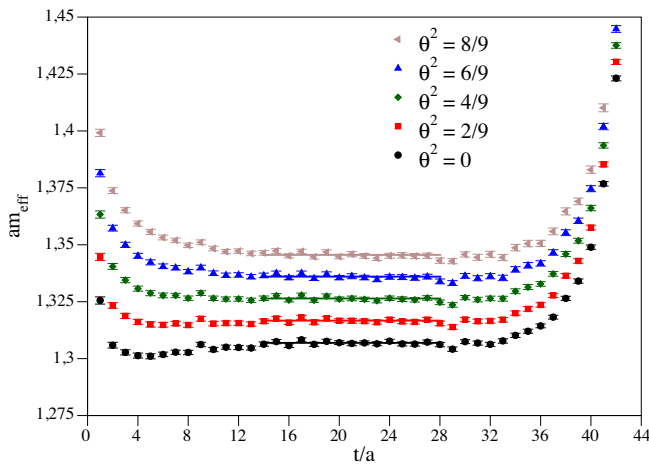


FIG. 1. Effective mass plots of the  $\eta_c$  meson with the fit of Eq. (3) for the ensemble H101.

To determine  $c^2$  and our masses  $am$ , we will fit the  $\eta_c$  and  $J/\psi$  correlators to the following form:

$$C(p, t) = A(1 + p^2(D + p^2E)) \left( e^{-t\sqrt{(am)^2 + c^2(ap)^2}} + B e^{-(L_T - t)\sqrt{(am)^2 + c^2(ap)^2}} \right), \quad (3)$$

with free parameters  $A$ ,  $am$ ,  $D$ ,  $E$ , and  $c^2$ —the speed of light squared. The parameter  $B$  takes the value of 1 if the gauge field has a periodic temporal boundary and 0 if it is open. An example of our tuning and the fit to Eq. (3) for the  $\eta_c$  correlator on the ensemble H101 is shown in Fig. 1.

## C. Chosen measurements and correlation functions

To make sure that we are using observables that are sensitive to all of the parameters in the RHQ action, we will be using both S- and P-wave charmonium ground-state masses (listed in Table II) in addition to the dispersion relation for the spin-averaged S-wave ground state. A possibility that would make this dependence a bit more obvious would have been to focus on the 1S hyperfine splitting, along with the S-wave–P-wave splitting, the spin-orbit splitting, and the tensor splitting within the P wave, as, for example, used in Refs. [9,26]. For computational reasons, we instead restrict the interpolator basis to the states that can be reached using the quark-line connected contractions of the simple mesonic operators at rest:

$$O(x) = (\bar{\psi}\Gamma\psi)(x) \quad (4)$$

and compare these directly with their continuum analogs. Note that the  $J^{PC} = 1^{+-}$   $h_c$  is, however, a good proxy for

TABLE II. List of operators used in our measurement of charmonium, their expected quantum number equivalents to continuum states, and the experimental masses of these states [46].

State	$\eta_c$	$J/\psi$	$\chi_{c0}$	$\chi_{c1}$	$h_c$
$\Gamma$	$\gamma_5$	$\gamma_i$	$I$	$\gamma_i\gamma_t$	$\gamma_i\gamma_j$
$J^{PC}$	$0^{-+}$	$1^{--}$	$0^{++}$	$1^{++}$	$1^{+-}$
Experiment [GeV]	2.9839	3.096916	3.41471	3.51072	3.52549

the spin average of the 1P states, as the 1P hyperfine splitting is expected to be very small [45] (which can also be seen in a previous lattice determination [26]). Throughout, we will use gauge-fixed wall sources with Gaussian sink smearing implemented by the method discussed in Appendix B to optimize for the ground states and those with twisting. An example of our zero-momentum states can be found in Fig. 2 for the ensemble N202.

For the open-boundary ensembles, we perform a single wall-source propagator inversion at  $T/2$ , in the middle of the bulk, and symmetrize the resulting correlator. We must make sure to not perform our fits too close to the open boundary, as these boundary effects can be relatively strong, as seen in Fig. 1.

#### D. Neural-network charm-action tuning

Our idea is to randomly choose values of  $\kappa_c$ ,  $r_s$ ,  $\nu$ ,  $c_E$ , and  $c_B$  and measure the basic spectrum of Table II on a sufficient number of gauge configurations. We will then train a neural network in predicting these parameters for given input masses and  $c^2$  and finally use this model to predict the best guesses for the parameters of the action that lie closest to the experimental masses with spin-averaged  $c^2 = 1$ , hopefully within a precision of 1%. We acknowledge that all of the states will likely have residual cutoff

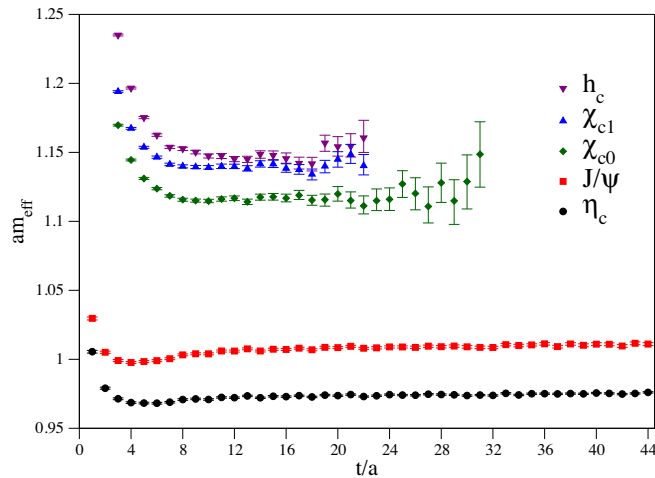


FIG. 2. Effective masses of the states listed in Table II for the ensemble N202.

effects with different slopes, but the parameters of the action should be able to absorb the leading cutoff effects [7,8]. As we approach the (chiral-)continuum limit, the states from the predicted parameters tend to the continuum masses, by design.

We strived to have at least about 30 different sets of run parameters randomly drawn from initially broad Gaussian distributions per ensemble [47]. For some ensembles, we performed more runs to investigate the possible inter-ensemble dependencies, such as those emanating from the pion mass or the volume. Typically, after about 20 runs, we start refining our parameter space by narrowing the new trial parameters and by feeding guesses back into the system to accelerate convergence. For each state entering the network, we use 1000 bootstraps, which will both help give the network lots of data to train against and inform it of correlations between states.

We will first consider each individual ensemble separately to train the network, eventually investigating combinations of ensembles and performing more-global fits. We initially have six input parameters: the lattice determinations of the  $\eta_c$ ,  $J/\psi$ ,  $\chi_{c0}$ ,  $\chi_{c1}$ , and  $h_c$  mesons and the lattice  $\eta_c - J/\psi$  spin-averaged dispersion relation  $c^2$ . We will use a feed-forward network with one hidden layer of only 12 neurons [48] and an output layer of five neurons ( $\kappa_c$ ,  $r_s$ ,  $\nu$ ,  $c_E$ , and  $c_B$ ). On each of the layers we use the sigmoid activation [49] and the Adam [50] minimizer, with an adjusted learning rate, early stopping, and a batch size of 80, with the loss function set as the mean-squared deviation. Often, the model will converge rapidly to stable training and validation losses in fewer than 200 epochs.

Once the network *understands* the relation between the lattice-determined states and the charm-action parameters on an ensemble, we determine the best finite-lattice-spacing approximation to the action parameters needed to obtain something close to the experimental states with  $c^2 = 1$  from the spin-averaged dispersion relation. Initial studies indicated that this approach gave predictions with heavier-than-physical  $\eta_c$  and  $\chi_{c0}$  states on our coarsest ensembles, and we decided to introduce so-called “class weights” to tell the network to prefer tuning  $\kappa_c$  by a factor of 2 compared to the other outputs. Empirically, this makes the  $\eta_c$  and  $\chi_{c0}$  closer to physical while making the  $\chi_{c1}$  and  $h_c$  and  $c^2$  a little less accurate, as will be seen in Fig. 4.

For the selection of our training and validation sets, we randomly shuffle the runs and remove approximately 20% for validation. We run the training over 50 of these reshufflings and perform a weighted average (with weight proportional to the inverse of the validation loss) of the networks’ best guesses to determine our predictions. In the following (Table III), we quote our predicted parameters with  $1\sigma$  errors, although this should not be construed as a true error but rather an indication of the variation of the parameters within the training runs we performed.

TABLE III. Charm-action parameter predictions for our data—the quantities in brackets are one-sigma variations in the predicted parameters; see the text for details. “Comb” refers to the prediction from the neural network when combining all results with a given lattice spacing. Different lattice spacings are separated by vertical spaces.

Ensemble	Runs	$\kappa_c$	$c_E$	$c_B$	$r_s$	$\nu$
A653	41	0.10951(09)	2.150(16)	2.313(28)	1.1645(34)	1.1515(40)
A654	33	0.10939(06)	2.110(11)	2.290(13)	1.1709(39)	1.1609(24)
Comb	74	0.10946(04)	2.138(09)	2.305(13)	1.1672(23)	1.1563(25)
U103	40	0.11409(09)	1.982(06)	2.139(15)	1.1375(13)	1.1229(16)
H101	40	0.11436(10)	1.925(11)	2.112(18)	1.1412(22)	1.1222(16)
H102	45	0.11447(07)	1.894(12)	2.032(16)	1.1454(20)	1.1098(28)
H105	40	0.11450(09)	1.937(08)	2.093(09)	1.1376(22)	1.1144(19)
Comb	165	0.11434(06)	1.940(07)	2.102(12)	1.1395(18)	1.1167(23)
B450	34	0.11826(10)	1.890(08)	2.051(08)	1.1017(23)	1.0849(36)
S400	35	0.11796(09)	1.880(10)	2.060(12)	1.1073(17)	1.0924(19)
N451	23	0.11835(10)	1.907(09)	2.025(07)	1.1020(15)	1.0950(20)
Comb	92	0.11810(04)	1.894(04)	2.052(05)	1.1043(12)	1.0926(12)
H200	36	0.12248(11)	1.864(09)	1.894(07)	1.0683(22)	1.0518(29)
N202	36	0.12256(20)	1.865(08)	1.889(10)	1.0679(13)	1.0446(24)
N203	36	0.12232(06)	1.863(09)	1.879(11)	1.0733(09)	1.0605(11)
N200	36	0.12211(09)	1.860(08)	1.888(06)	1.0753(09)	1.0564(15)
Comb	144	0.12235(05)	1.859(05)	1.886(04)	1.0722(09)	1.0552(08)
N300	50	0.12608(15)	1.792(15)	1.873(14)	1.0382(13)	1.0168(19)

## IV. RESULTS

### A. Table of predictions

In Table III, we present our results for the tuning on individual ensembles as well as a combined dataset built from the individual ones at fixed lattice spacing, which is practically an assumption of a flat approach to physical light and strange quark masses, combined with the (likely justified) assumption that finite-volume effects in our charmonium observables are not relevant for our volumes. Typically, the loss from the neural network reduces when the larger dataset “Comb” is used, and this larger dataset should protect us a little more from overfitting.

We perform a correlated single-exponential  $\chi^2$ -minimization fit to each individual state in Table II for each run to determine the masses of these states, with fit ranges chosen appropriately to give  $\chi^2/\text{d.o.f.}$  of the order of 1 with  $0.05 < p < 0.95$ , over as large a range of time slices as possible. For example, for the prediction for N202 (Fig. 2), we fit the range  $t/a = 20 \rightarrow 32$  for the  $\eta_c$  and  $J/\psi$ ,  $t/a = 7 \rightarrow 32$  for the  $\chi_{c0}$  and  $\chi_{c1}$ , and  $t/a = 9 \rightarrow 23$  for the  $h_c$ . These masses, along with the spin-averaged effective speed of light squared, are then fed into the neural network to learn the parameter dependence on the states. We see good stability with the neural-network-predicted parameters upon variation of our fit ranges.

Comparing our results to the similar tuning of Ref. [28] ( $\kappa_c = 0.10959947$ ,  $c_E = 1.7819512$ ,  $c_B = 1.9849139$ ,  $r_s = 1.1881607$ , and  $\nu = 1.1450511$ ) albeit on different ensembles,

we see some similarities and a few differences. Namely, that at a similar lattice spacing to theirs ( $a^{-1} = 2.194 \text{ GeV}$ ), our 1-ensembles, the values we obtain for  $\kappa_c$ ,  $c_E$ , and  $c_B$  are larger, while both  $r_s$  and  $\nu$  are smaller. Our larger values of  $c_E$  and  $c_B$  are unsurprising, as the gauge fields used are generated with the tree-level Symanzik gauge action whereas they used the Iwasaki, and the size of the non-perturbative  $c_{\text{SW}}$  is larger for the Symanzik gauge action at comparable lattice spacing. It is interesting to note that their

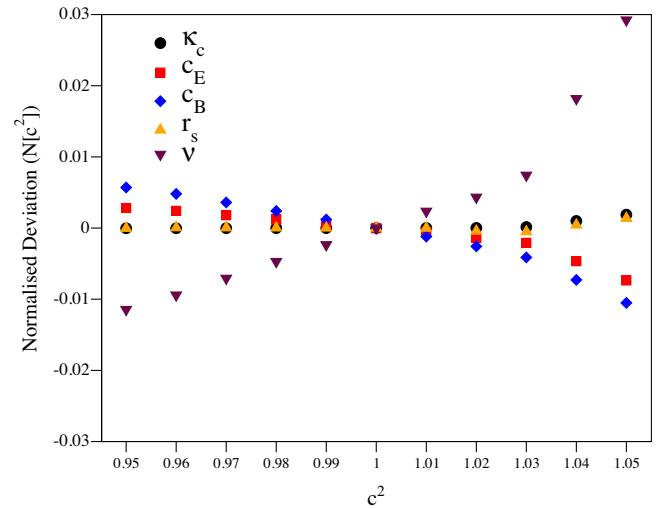


FIG. 3. The predicted normalized deviation of the parameters as we change the effective spin-averaged speed of light.

values for  $\kappa_c$ ,  $r_s$ , and  $\nu$  resemble more our tuning parameters on the coarser ensembles A653 and A654.

It is clear from Table III that as the lattice spacing reduces the size of all of the parameters  $c_E$ ,  $c_B$ ,  $r_s$ , and  $\nu$  also decrease, with  $r_s$  and  $\nu$  practically tending to their expected continuum values of 1. Both of the parameters  $c_E$  and  $c_B$  are greater than the value of (but tending toward)  $c_{\text{SW}}$  from Ref. [51], with the hierarchy of  $c_B > c_E$  as expected perturbatively from Ref. [25].

## B. Can we tune parameters independently of others?

As  $c^2 = 1$  from the spin-averaged dispersion relation is one of our inputs, we can use this as a handle and investigate the dependence on the predicted *physical* parameters as this value is varied (and all the other states are still set to their physical values). If the deviation on  $\kappa_c$ ,  $r_s$ ,  $c_E$ ,  $c_B$ , and  $\nu$  is large as small changes are applied to this dispersion relation, then the model is suggesting that there is significant interdependence between these parameters

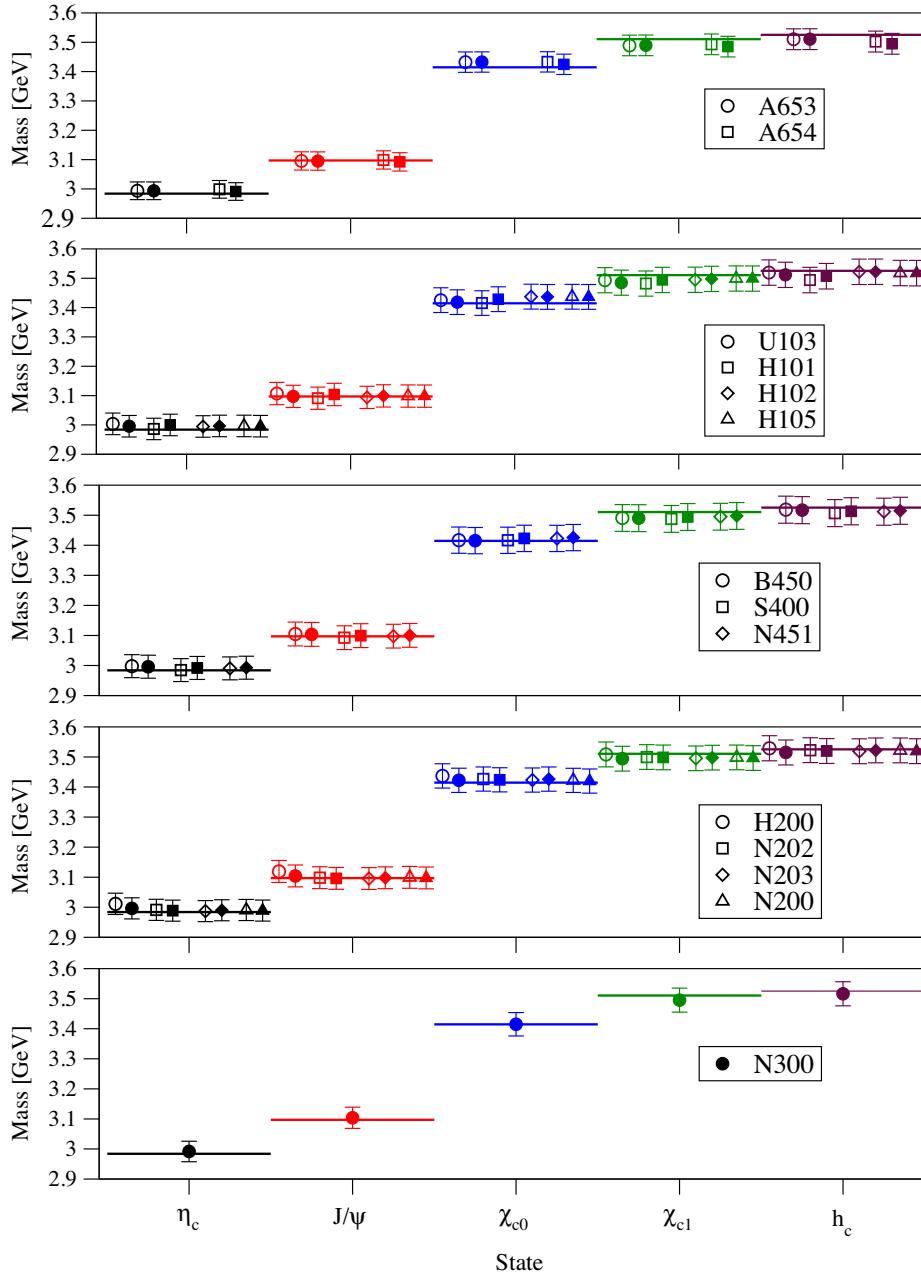


FIG. 4. Overview of the resulting masses for the hadrons used for our neural net tuning. The horizontal lines show the experiment masses. The uncertainty combines statistical and scale-setting uncertainties in quadrature, and the uncertainty is dominated by the scale setting. The panels are sorted from coarsest (top) to finest (bottom) lattice spacing. For each ensemble, two results are shown: the tuning on the single ensemble (left, open symbol) and the tuning on the collection of ensembles with the same  $\beta$  (right, filled symbol). Ensembles within the same panel differ by volume and/or pion mass.

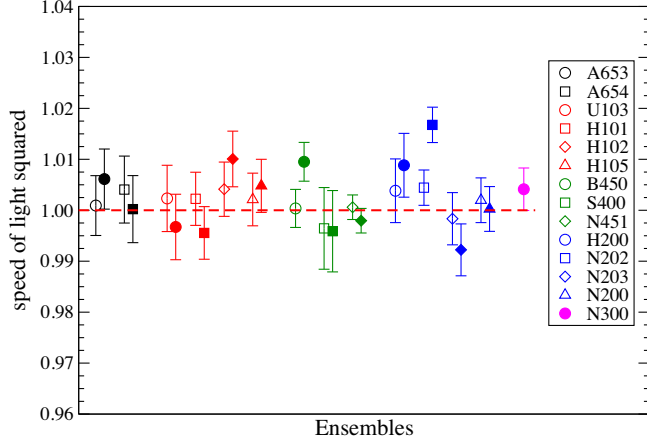


FIG. 5. Spin-averaged  $c^2$  reached through our tuning prescription. For each ensemble, a pair of data points is shown. The left (open) data point results from the tuning on the single ensemble, while the right (filled) data point results from the tuning using all ensembles with the same lattice spacing.

and that this tuning should not be done independently, as was performed in Ref. [28].

Figure 3 illustrates the normalized deviation for some model-predicted parameter  $P$ , which we define as

$$N[c^2] = (P[c^2] - P[1])/P[1], \quad (5)$$

for the combined A653 and A654 ensembles as we varied the spin-averaged dispersion relation's  $c^2$ . We can see that  $\kappa_c$  and  $r_s$  do not depend strongly on  $c^2$ , whereas  $\nu$ ,  $c_E$ , and  $c_B$  do, with  $c_E$  and  $c_B$  being somewhat anticorrelated with  $\nu$ . Although  $\nu$  seems to be the main perpetrator in determining the effective speed of light,  $c_E$  and  $c_B$  both

change accordingly and would likely need to be retuned to accommodate an independent tuning in  $\nu$ .

### C. Accuracy of our predictions and systematics

We now proceed to test our predicted parameters from Table III by performing the same measurement runs on the same configurations as the training was performed on and comparing the determined states and the effective speed of light to the physical continuum states. We will investigate both the combined and the individual results to illustrate the lack of measurable dependence on the pion mass within the precision of our determinations. A plot of our ability to reproduce the spectrum is shown in Fig. 4, and one can see that within our large errors there is good agreement; mostly this is due to the lack of precision of our lattice spacing.

Figure 5 shows the spin-averaged  $c^2$  reached for our tuning procedure on all ensembles. For each ensemble, we show both the result from the tuning procedure on a single ensemble (the left point of the pair) and the result from using all ensembles at the same value of  $\beta$  (the right point of a given pair). Our overall goal here was to obtain  $c^2 = 1$  to about 1%, which we achieve on most ensembles for the spin average, or the individual  $\eta_c$  and  $J/\psi$ . For the dispersion relation, the single-ensemble tuning works a bit better than combining ensembles at each lattice spacing. However, the opposite will be true for the splitting discussed in the next few paragraphs. Note that, while there are some outliers, the situation is vastly improved compared to a standard Wilson action ( $c_B = c_E = c_{sw}$ , and  $r_s = r_t = \nu = 1$ ) as used for the charm quark in Ref. [6] and discussed in the next subsection (Sec. IV D). The individual determinations of  $c^2$  for the  $\eta_c$  and  $J/\Psi$  can be found in Fig. 8 in the appendixes. We note that all of our  $\eta_c$

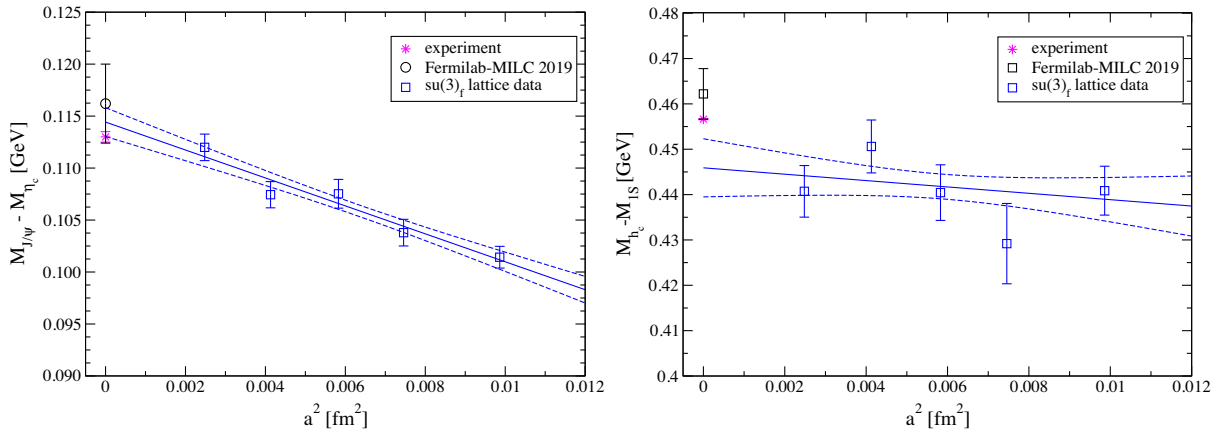


FIG. 6. Left panel: 1S hyperfine splitting on the trajectory with  $m_u/d = m_s$  corresponding to the heaviest pion masses (choosing the largest volume) in Table I. The splitting is clearly tending toward the physical splitting for small lattice spacing. The blue lines and blue dashed error band show the results of a fit linear in the lattice spacing squared, which is compatible with the presence of such subleading discretization effects in our action. Right panel: a proxy for the S-wave–P-wave splitting along the same line. Note that both results are not determinations and instead illustrate the quality and suitability of our tuning.

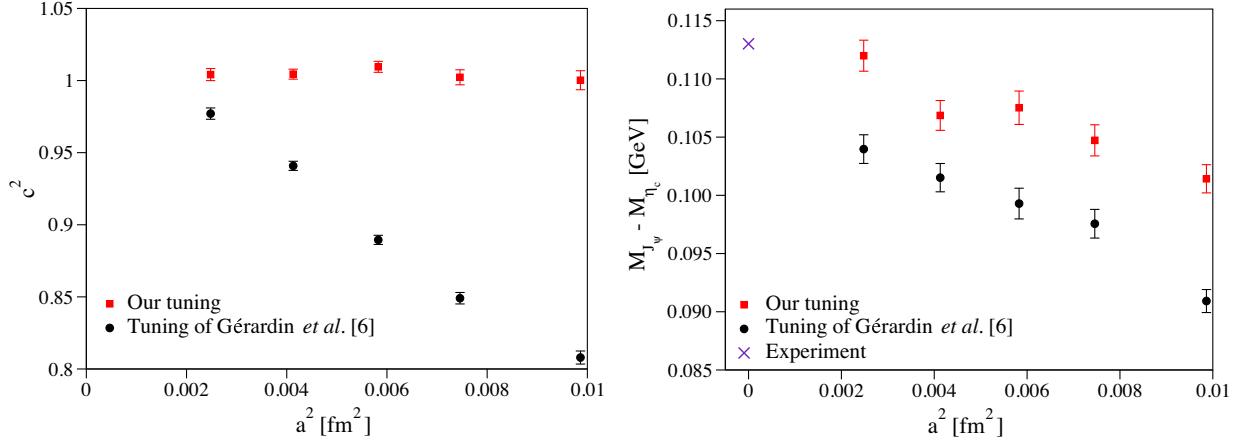


FIG. 7. Left: the speed of light squared from the spin-averaged dispersion relation using either the charm-quark tuning of Ref. [6] or our tuning on ensembles at the  $SU(3)_f$ -symmetric point. Right: the hyperfine splitting for the two tunings.

values of  $c^2$  lie below those of the  $J/\Psi$  and their difference is at most of the order of 2% for our data. There is a suggestion that this difference becomes smaller with decreasing pion mass and increased physical volume.

To investigate residual discretization effects within our approach, we take a look at the mass splittings among our tuning states. In the left-hand-side panel in Fig. 6, we show the 1S hyperfine splitting between the  $J/\psi$  and  $\eta_c$  mesons resulting from the neural net training with all ensembles at a given value of  $\beta$ . While the run parameters suggested by the neural net based on the training data do not lead to a particularly accurate 1S hyperfine splitting at coarse lattice spacing, this discrepancy does get smaller toward the continuum limit. This suggests that our strategy of using the physical inputs for the tuning of the action parameters at each lattice spacing is working. In addition to the data from our final runs, we also show the PDG value [46] as a magenta star and an independent lattice determination that provides this splitting as a prediction [26]. For a plot of further results for this quantity, see Fig. 8 of the same reference.

The right-hand side of Fig. 6 shows a mass splitting which is equal to the S-wave–P-wave splitting in the absence of a P-wave hyperfine splitting. In this quantity, we expect a very mild heavy-quark dependence, as the physical S-wave–P-wave splittings in charmonium and bottomonium are almost the same. Just like for the hyperfine splitting, there is no obvious sign of issues with our tuning approach. Overall, we tend to get somewhat smaller values for this splitting, although with large errors coming from our determination of  $h_c$ . As our application for this action will mostly be qualitative studies of hadron-hadron scattering, we currently see no need to attempt to further improve the observed behavior, which would require an improvement in statistical precision on our side combined with an improvement in the determination of the lattice spacing.

#### D. A tuning comparison on the same ensembles

In Ref. [6], a charm-quark tuning was performed that uses  $c_E = c_B = c_{SW}$  and  $r_s = \nu = 1$ , varying  $\kappa_c$  to achieve the physical continuum value of the  $D_s$ -meson mass on the same ensembles as used in this work. This tuning treats the charm quark on the same footing as the light and strange quarks by using the standard Wilson-clover action; one may well expect this to have significant discretization effects as  $aM_{\eta_c}$  becomes of the order of 1 for the coarse ensembles.

Figure 7 illustrates the deviation of the spin-averaged dispersion relation  $c^2$ , which can be used as a proxy for the magnitude of discretization effects of both tunings. In the dispersion relation for the  $D_s$  tuning, the deviation from 1 is at most 20%, reducing to about 4% on the finest (N300) lattice. A naive, straight-line fit through all of the  $D_s$ -tuned results describes the data poorly and overpredicts the value of  $c^2$  in the continuum as there is still some visible curvature at small  $a^2$ . A quadratic fit in  $a^2$  to the three finest ensembles describes the data well and gives  $c^2 = 1$  in continuum.

The hyperfine splitting in Fig. 7 shows a similar slope in  $a^2$  between the two approaches, although the  $D_s$  tuning lies systematically below that of our tuning and the physical hyperfine splitting. This is due to the ensembles used in this comparison lying at the  $SU(3)_f$ -symmetric point and the  $D_s$  tuning compensating for the valence strange being lighter than its physical value. This has the side effect that a precise charm tuning via the  $D_s$  is valid only at the physical point or through extrapolations toward it when the strange-quark mass is unphysical.

## V. CONCLUSIONS AND OUTLOOK

We have shown that it is possible to nonperturbatively determine charm-quark action parameters reasonably precisely using machine learning techniques. This method is appealing as it does not rely on lattice perturbation theory or

an underlying model to tune parameters. Its main drawback is that a sufficiently large number of measurement runs need to be made for training purposes, which could make it costly for large ensembles. Although, at the precision we are able to achieve, we see little pion-mass or finite-volume dependence of our tuning parameters. We also note that it appears impossible to exactly reproduce the chosen continuum states of charmonium at finite lattice spacing with this five-parameter action, even though a good approximation can be achieved.

We see no reason why this approach could not be extended to, for example, b-quark physics using the same relativistic heavy-quark action or any of the fewer-parameter variants. While residual discretization effects are expected to be sizable for bottomonium [8], this approach should be very useful for refining some older predictions for exotic hadrons in the  $B$ -meson spectrum [14]. The same approach could equally well be used to tune an effective action, such as NRQCD, provided one has enough continuum states to compare against that allow for a handle on the underlying simulation parameters. The method presented here, quite naturally, extends to even higher-order heavy-quark actions due to the inherent flexibility of neural-network fits.

In future works, we will use this action for scattering studies using Lüscher’s finite-volume method for heavy-light meson spectroscopy and charmonium spectroscopy, with the stochastic distillation technique [52,53]. In this regard, a first step consists of testing the dispersion relations of heavy-light  $D$  and  $D_s$  mesons in our approach.

### ACKNOWLEDGMENTS

The authors acknowledge useful discussions with Christopher Johnson and Matthias Lutz and are grateful to Sasa Prelovsek for her useful comments on a first draft. D. M. acknowledges funding by the Heisenberg Programme of the Deutsche Forschungsgemeinschaft (DFG, German Research Foundation)—Project No. 454605793. R. J. H. by the European Research Council (ERC) under the European Unions Horizon 2020 research and innovation program through Grant Agreement No. 771971-SIMDAMA. Calculations for this project were partly performed on the HPC cluster “Mogon II” at JGU Mainz. This research was supported in part by the cluster computing resource provided by the IT Division at the GSI Helmholtzzentrum für Schwerionenforschung, Darmstadt, Germany (HPC cluster Virgo). The simulations were partly performed on the national supercomputer HPE Apollo Hawk at the High Performance Computing Center Stuttgart (HLRS) under acronym RinQCD4PANDA. For the neural-network training and predictions, we made use of the Keras API.

### APPENDIX A: ON OUR CHARM-ACTION IMPLEMENTATION

We use a modified version of the library OpenQCD-1.6 [38] for our computation of propagators for the charm-

quark Dirac operator of Eq. (1). This required the rewriting of the Dirac operator in single and double precision in Advanced Vector Extensions and fused multiply-add vector intrinsics, as some of the optimizations (and inline assembly) used in the implementation of the *vanilla* Wilson action could not be utilized. On paper, the arithmetic intensity of this charm action is about a factor of 2 more expensive than the usual Wilson action, although an optimization was used here to turn the underlying spinors into color-major, spin-minor order (OpenQCD-1.6 is spin-major, color-minor) to improve cache coherence and perform fewer shuffling and register loading operations. It is likely that this charm-quark action is worse conditioned than the usual Wilson action, as it is found to have a larger clover term than  $c_{\text{SW}}$ . Nevertheless, our implementation is roughly comparable to a valence strange-quark inversion at physical  $m_s$  [40] in OpenQCD using the DFL\_SAP\_GCR algorithm [54].

In initial investigations, we found some deviations between charmonium correlators at large times due to the stopping condition of the  $L_2$ -norm of the residual depending on the precision we used. To help resolve this, we changed the stopping criteria to be the  $L_\infty$ -norm instead, which empirically behaved much better.

### APPENDIX B: COULOMB GAUGE-FIXED BOX SINKS AS A SINK SMEARING

If we consider the box-sink propagator introduced in Ref. [40],

$$\tilde{S}(x, t) = \sum_{r=0}^{r^2 < R^2} S(x + r, t), \quad (\text{B1})$$

when one goes to compute the contracted meson, there are clearly double sums, and, in the limit of  $R^2 \rightarrow 3\frac{L^2}{2}$ , we are performing two sums over the spatial volume, which becomes very expensive. Empirically, we find the cost in contractions scales quadratically with  $R^2$ , and this sum quickly becomes the dominant cost of contractions as  $R^2$  increases.

A more-efficient implementation would be to notice that the box-sink approach could be considered as a convolution with a particular step function,  $f(x) = \theta(r < R^2)$ , and herein lies the connection to sink smearing and a clue to efficient calculation of these propagators. An approximation to this step function could be a Gaussian with some width  $\sigma \propto R^2$ ,  $f(x) = e^{-x^2/\sigma}$  (although, in principle, any arbitrary function could be used, for S-wave states something with rotational symmetry makes sense), and we apply the convolution using the usual (fast) Fourier transform prescription:

$$S(p, t) = \mathcal{F}(S(x, t)) = \sum_x e^{ip \cdot x} S(x, t), \quad (\text{B2})$$

where  $\mathcal{F}$  is used to denote the Fourier transform and likewise  $\mathcal{F}^{-1}$  its inverse.

$$\bar{S}(x) = \frac{1}{V} \mathcal{F}^{-1}(S(p, t) f^*(p)). \quad (\text{B3})$$

We have turned a somewhat expensive approximate convolution into a full convolution with an arbitrary function  $f(x)$ , the cost of which are  $12 \times 12$  complex spatial-volume FFTs per time slice.

It is important to note that this approach holds only because of the Coulomb gauge-fixed wall sources we use, as only in this case can one treat the links as identity matrices and, hence, completely ignore them and apply a continuous function. Such approaches have been known in the literature in the case of smearing either the source and/or the sink, e.g., applying arbitrary potentials in Ref. [55].

### APPENDIX C: $c^2$ FROM THE INDIVIDUAL PSEUDOSCALAR AND VECTOR CHANNELS

Figure 8 shows the speed of light squared for the individual  $J/\psi$  and  $\eta_c$  mesons. The value for the  $J/\psi$  is

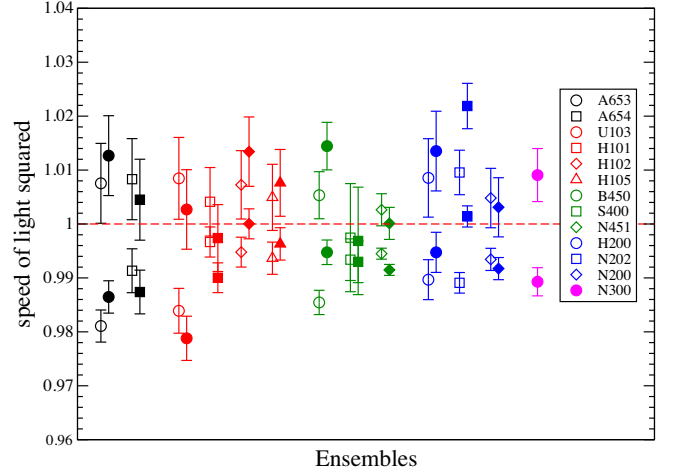


FIG. 8. The same as Fig. 5, only with the individual  $\eta_c$  (bottom points) and  $J/\Psi$  (top points) values of  $c^2$  instead of their spin average.

typically a bit larger than that of the  $\eta_c$  and both individually show only a small deviation from the relativistic speed of light.

- 
- [1] M. Lüscher, Volume dependence of the energy spectrum in massive quantum field theories. 2. Scattering states, *Commun. Math. Phys.* **105**, 153 (1986).
- [2] M. Lüscher, Two particle states on a torus and their relation to the scattering matrix, *Nucl. Phys.* **B354**, 531 (1991).
- [3] R. A. Briceño, J. J. Dudek, and R. D. Young, Scattering processes and resonances from lattice QCD, *Rev. Mod. Phys.* **90**, 025001 (2018).
- [4] M. Bruno *et al.*, Simulation of QCD with  $N_f = 2 + 1$  flavors of non-perturbatively improved Wilson fermions, *J. High Energy Phys.* **02** (2015) 043.
- [5] B. Sheikholeslami and R. Wohlert, Improved continuum limit lattice action for QCD with Wilson fermions, *Nucl. Phys.* **B259**, 572 (1985).
- [6] A. Gérardin, M. Cè, G. von Hippel, B. Hörz, H. B. Meyer, D. Mohler, K. Ottnad, J. Wilhelm, and H. Wittig, The leading hadronic contribution to  $(g-2)_\mu$  from lattice QCD with  $N_f = 2 + 1$  flavours of  $O(a)$  improved Wilson quarks, *Phys. Rev. D* **100**, 014510 (2019).
- [7] A. X. El-Khadra, A. S. Kronfeld, and P. B. Mackenzie, Massive fermions in lattice gauge theory, *Phys. Rev. D* **55**, 3933 (1997).
- [8] M. B. Oktay and A. S. Kronfeld, New lattice action for heavy quarks, *Phys. Rev. D* **78**, 014504 (2008).
- [9] T. Burch, C. DeTar, M. Di Pierro, A. X. El-Khadra, E. D. Freeland, S. Gottlieb, A. S. Kronfeld, L. Levkova, P. B. Mackenzie, and J. N. Simone, Quarkonium mass splittings in three-flavor lattice QCD, *Phys. Rev. D* **81**, 034508 (2010).
- [10] C. Bernard *et al.* (Fermilab Lattice and MILC Collaborations), Tuning Fermilab heavy quarks in  $2 + 1$  flavor lattice QCD with application to hyperfine splittings, *Phys. Rev. D* **83**, 034503 (2011).
- [11] J. A. Bailey *et al.* (Fermilab Lattice and MILC Collaborations), Update of  $|V_{cb}|$  from the  $\bar{B} \rightarrow D^* \ell \bar{\nu}$  form factor at zero recoil with three-flavor lattice QCD, *Phys. Rev. D* **89**, 114504 (2014).
- [12] D. Mohler, C. B. Lang, L. Leskovec, S. Prelovsek, and R. M. Woloshyn,  $D_{s0}^*(2317)$  Meson and  $D$ -Meson-Kaon Scattering from Lattice QCD, *Phys. Rev. Lett.* **111**, 222001 (2013).
- [13] C. B. Lang, L. Leskovec, D. Mohler, S. Prelovsek, and R. M. Woloshyn,  $D_s$  mesons with DK and  $D^*K$  scattering near threshold, *Phys. Rev. D* **90**, 034510 (2014).
- [14] C. B. Lang, D. Mohler, S. Prelovsek, and R. M. Woloshyn, Predicting positive parity  $B_s$  mesons from lattice QCD, *Phys. Lett. B* **750**, 17 (2015).
- [15] C. B. Lang, L. Leskovec, D. Mohler, and S. Prelovsek, Vector and scalar charmonium resonances with lattice QCD, *J. High Energy Phys.* **09** (2015) 089.
- [16] S. Piemonte, S. Collins, D. Mohler, M. Padmanath, and S. Prelovsek, Charmonium resonances with  $J^{PC} = 1^{--}$  and  $3^{--}$  from  $\bar{D}D$  scattering on the lattice, *Phys. Rev. D* **100**, 074505 (2019).
- [17] S. Prelovsek, S. Collins, D. Mohler, M. Padmanath, and S. Piemonte, Charmonium-like resonances with  $J^{PC} = 0^{++}$ ,  $2^{++}$  in coupled  $\bar{D}\bar{D}$ ,  $D_s\bar{D}_s$  scattering on the lattice, *J. High Energy Phys.* **06** (2021) 035.

- [18] For a more thorough description of this procedure, see Sec. IV B in Ref. [16].
- [19] G. Moir, M. Peardon, S. M. Ryan, C. E. Thomas, and D. J. Wilson, Coupled-channel  $D\pi$ ,  $D\eta$  and  $D_s\bar{K}$  scattering from lattice QCD, *J. High Energy Phys.* **10** (2016) 011.
- [20] G. K. C. Cheung, C. O'Hara, G. Moir, M. Peardon, S. M. Ryan, C. E. Thomas, and D. Tims (Hadron Spectrum Collaboration), Excited and exotic charmonium,  $D_s$  and  $D$  meson spectra for two light quark masses from lattice QCD, *J. High Energy Phys.* **12** (2016) 089.
- [21] G. K. C. Cheung, C. E. Thomas, J. J. Dudek, and R. G. Edwards (Hadron Spectrum Collaboration), Tetraquark operators in lattice QCD and exotic flavour states in the charm sector, *J. High Energy Phys.* **11** (2017) 033.
- [22] G. K. C. Cheung, C. E. Thomas, D. J. Wilson, G. Moir, M. Peardon, and S. M. Ryan (Hadron Spectrum Collaboration),  $DK\ I = 0, D\bar{K}I = 0, 1$  scattering and the  $D_{s0}^*(2317)$  from lattice QCD, *J. High Energy Phys.* **02** (2021) 100.
- [23] L. Gayer, N. Lang, S. M. Ryan, D. Tims, C. E. Thomas, and D. J. Wilson (Hadron Spectrum Collaboration), Isospin-1/2  $D\pi$  scattering and the lightest  $D_0^*$  resonance from lattice QCD, *J. High Energy Phys.* **07** (2021) 123.
- [24] S. Aoki, Y. Kuramashi, and S.-i. Tominaga, Relativistic heavy quarks on the lattice, *Prog. Theor. Phys.* **109**, 383 (2003).
- [25] S. Aoki, Y. Kayaba, and Y. Kuramashi, A perturbative determination of mass dependent  $O(a)$  improvement coefficients in a relativistic heavy quark action, *Nucl. Phys.* **B697**, 271 (2004).
- [26] C. DeTar, A. S. Kronfeld, S.-h. Lee, D. Mohler, and J. N. Simone (Fermilab Lattice and MILC Collaborations), Splittings of low-lying charmonium masses at the physical point, *Phys. Rev. D* **99**, 034509 (2019).
- [27] J. A. Bailey, C. DeTar, Y.-C. Jang, A. S. Kronfeld, W. Lee, and M. B. Oktay, Heavy-quark meson spectrum tests of the Oktay-Kronfeld action, *Eur. Phys. J. C* **77**, 768 (2017).
- [28] Y. Namekawa *et al.* (PACS-CS Collaboration), Charm quark system at the physical point of  $2 + 1$  flavor lattice QCD, *Phys. Rev. D* **84**, 074505 (2011).
- [29] Y. Namekawa *et al.* (PACS-CS Collaboration), Charmed baryons at the physical point in  $2 + 1$  flavor lattice QCD, *Phys. Rev. D* **87**, 094512 (2013).
- [30] And similarly for Ref. [31] except for the tuning in  $\nu$ .
- [31] Y. Kayaba, S. Aoki, M. Fukugita, Y. Iwasaki, K. Kanaya, Y. Kuramashi, M. Okawa, A. Ukawa, and T. Yoshié (CP-PACS Collaboration), First nonperturbative test of a relativistic heavy quark action in quenched lattice QCD, *J. High Energy Phys.* **02** (2007) 019.
- [32] S. Aoki *et al.* (CP-PACS and JLQCD Collaborations), Non-perturbative  $O(a)$  improvement of the Wilson quark action with the RG-improved gauge action using the Schrödinger functional method, *Phys. Rev. D* **73**, 034501 (2006).
- [33] H.-W. Lin and N. Christ, Non-perturbatively determined relativistic heavy quark action, *Phys. Rev. D* **76**, 074506 (2007).
- [34] A similar approach for  $B$  physics can be found in Ref. [35].
- [35] Y. Aoki, N. H. Christ, J. M. Flynn, T. Izubuchi, C. Lehner, M. Li, H. Peng, A. Soni, R. S. Van de Water, and O. Witzel (RBC and UKQCD Collaborations), Nonperturbative tuning of an improved relativistic heavy-quark action with application to bottom spectroscopy, *Phys. Rev. D* **86**, 116003 (2012).
- [36] N. H. Christ, M. Li, and H.-W. Lin, Relativistic heavy quark effective action, *Phys. Rev. D* **76**, 074505 (2007).
- [37] G. S. Bali, E. E. Scholz, J. Simeth, and W. Söldner (RQCD Collaboration), Lattice simulations with  $N_f = 2 + 1$  improved Wilson fermions at a fixed strange quark mass, *Phys. Rev. D* **94**, 074501 (2016).
- [38] M. Lüscher and S. Schaefer, Lattice QCD with open boundary conditions and twisted-mass reweighting, *Comput. Phys. Commun.* **184**, 519 (2013).
- [39] E.-H. Chao, R. J. Hudspith, A. Gérardin, J. R. Green, H. B. Meyer, and K. Ottnad, Hadronic light-by-light contribution to  $(g - 2)_\mu$  from lattice QCD: a complete calculation, *Eur. Phys. J. C* **81**, 651 (2021).
- [40] R. J. Hudspith, B. Colquhoun, A. Francis, R. Lewis, and K. Maltman, A lattice investigation of exotic tetraquark channels, *Phys. Rev. D* **102**, 114506 (2020).
- [41] Fixed to an accuracy of  $10^{-14}$  using the (Coulomb) Fourier-accelerated conjugate gradient (CFACG) algorithm [42] implemented in GLU.
- [42] R. J. Hudspith (RBC and UKQCD Collaborations), Fourier accelerated conjugate gradient lattice gauge fixing, *Comput. Phys. Commun.* **187**, 115 (2015).
- [43] P. F. Bedaque, Aharonov-Bohm effect and nucleon nucleon phase shifts on the lattice, *Phys. Lett. B* **593**, 82 (2004).
- [44] C. T. Sachrajda and G. Villadoro, Twisted boundary conditions in lattice simulations, *Phys. Lett. B* **609**, 73 (2005).
- [45] R. F. Lebed and E. S. Swanson, Quarkonium  $h$  states as arbiters of exoticity, *Phys. Rev. D* **96**, 056015 (2017).
- [46] P. Zyla *et al.* (Particle Data Group), Review of particle physics, *Prog. Theor. Exp. Phys.* **2020**, 083C01 (2020).
- [47] To start with, we draw values of  $c_E$  and  $c_B$  around  $c_{SW}$  with a bias toward larger values and a large width, as motivated by perturbation theory.  $\kappa_c$ ,  $r_s$ , and  $\nu$  are initially guessed from a linear fit in  $a^2$  from previously measured ensembles.
- [48] We tried many different numbers of layers and neurons in each layer. Enlarging these numbers either did not change predictions compared to the small, simple network or resulted in what we determined to be overfitting.
- [49] H. R. Wilson and J. D. Cowan, Excitatory and inhibitory interactions in localized populations of model neurons, *Biophys. J.* **12**, 1 (1972).
- [50] D. P. Kingma and J. Ba, Adam: A method for stochastic optimization, [arXiv:1412.6980](https://arxiv.org/abs/1412.6980).
- [51] J. Bulava and S. Schaefer, Improvement of  $N_f = 3$  lattice QCD with Wilson fermions and tree-level improved gauge action, *Nucl. Phys.* **B874**, 188 (2013).
- [52] M. Peardon, J. Bulava, J. Foley, C. Morningstar, J. Dudek, R. G. Edwards, B. Joo, H.-W. Lin, D. G. Richards, and K. J. Juge (Hadron Spectrum Collaboration), A novel quark-field creation operator construction for hadronic physics in lattice QCD, *Phys. Rev. D* **80**, 054506 (2009).
- [53] C. Morningstar, J. Bulava, J. Foley, K. J. Juge, D. Lenkner, M. Peardon, and C. H. Wong, Improved stochastic estimation of quark propagation with Laplacian heaviside smearing in lattice QCD, *Phys. Rev. D* **83**, 114505 (2011).
- [54] M. Lüscher, Local coherence and deflation of the low quark modes in lattice QCD, *J. High Energy Phys.* **07 07** (2007) 081.
- [55] C. T. H. Davies, K. Hornbostel, A. Langnau, G. P. Lepage, A. Lidsey, J. Shigemitsu, and J. H. Sloan, Precision Upsilon spectroscopy from nonrelativistic lattice QCD, *Phys. Rev. D* **50**, 6963 (1994).